

References and Notes

1. T. A. Rapoport, *Nature* **450**, 663 (2007).
2. R. S. Hegde, H. D. Bernstein, *Trends Biochem. Sci.* **31**, 563 (2006).
3. A. K. Veenendaal, C. van der Does, A. J. Driessens, *Biochim. Biophys. Acta* **1694**, 81 (2004).
4. C. W. Bowers, F. Lau, T. J. Silhavy, *J. Bacteriol.* **185**, 5697 (2003).
5. T. J. Silhavy, H. A. Shuman, J. Beckwith, M. Schwartz, *Proc. Natl. Acad. Sci. U.S.A.* **74**, 5411 (1977).
6. P. Bassford, T. J. Silhavy, J. Beckwith, *J. Bacteriol.* **139**, 19 (1979).
7. C. L. Cosma, P. N. Danese, J. H. Carlson, T. J. Silhavy, W. B. Snyder, *Mol. Microbiol.* **18**, 491 (1995).
8. W. B. Snyder, L. J. Davis, P. N. Danese, C. L. Cosma, T. J. Silhavy, *J. Bacteriol.* **177**, 4216 (1995).
9. N. L. Price, T. L. Raivio, *J. Bacteriol.* **191**, 1798 (2008).
10. K. Yamamoto, A. Ishihama, *Biosci. Biotechnol. Biochem.* **70**, 1688 (2006).
11. Materials and methods are available as supporting material on *Science Online*.
12. A. Kihara, Y. Akiyama, K. Ito, *Proc. Natl. Acad. Sci. U.S.A.* **92**, 4532 (1995).
13. A. Kihara, Y. Akiyama, K. Ito, *J. Mol. Biol.* **279**, 175 (1998).
14. T. Ogura *et al.*, *Mol. Microbiol.* **31**, 833 (1999).
15. C. Walsh, *Antibiotics: Actions, Origins, Resistance* (ASM Press, Washington, DC, 2003).
16. Y. Akiyama, K. Ito, *J. Biol. Chem.* **264**, 437 (1989).
17. W. E. Feldman, N. S. Manning, *Antimicrob. Agents Chemother.* **23**, 551 (1983).
18. J. J. Rahal Jr., M. S. Simberkoff, *Antimicrob. Agents Chemother.* **16**, 13 (1979).
19. Q. Xu, J. C. Reed, *Mol. Cell* **1**, 337 (1998).
20. H. J. Chae *et al.*, *Gene* **323**, 101 (2003).
21. M. I. Smith, M. Deshmukh, *Cell Death Differ.* **14**, 1011 (2007).
22. F. Lisbona *et al.*, *Mol. Cell* **33**, 679 (2009).
23. R. Huckleberry, *Apoptosis* **9**, 299 (2004).
24. We thank I. Collinson for SecY antisera and T. Ogura for strains. This work was supported by the National Institute of General Medical Sciences (T.J.S.), the New Jersey Commission on Cancer Research (J.V.S.), and the Canton de Genève and the Swiss National Science Foundation (F.S. and D.B.).

Supporting Online Material

www.sciencemag.org/cgi/content/full/325/5941/753/DC1

Materials and Methods

Figs. S1 to S3

Table S1

References

12 February 2009; accepted 23 June 2009
10.1126/science.1172221

Synaptic Integration in Tuft Dendrites of Layer 5 Pyramidal Neurons: A New Unifying Principle

Matthew E. Larkum,^{1,*†} Thomas Nevian,^{1,*} Maya Sandler,² Alon Polksky,² Jackie Schiller^{2†}

Tuft dendrites are the main target for feedback inputs innervating neocortical layer 5 pyramidal neurons, but their properties remain obscure. We report the existence of *N*-methyl-D-aspartate (NMDA) spikes in the fine distal tuft dendrites that otherwise did not support the initiation of calcium spikes. Both direct measurements and computer simulations showed that NMDA spikes are the dominant mechanism by which distal synaptic input leads to firing of the neuron and provide the substrate for complex parallel processing of top-down input arriving at the tuft. These data lead to a new unifying view of integration in pyramidal neurons in which all fine dendrites, basal and tuft, integrate inputs locally through the recruitment of NMDA receptor channels relative to the fixed apical calcium and axosomatic sodium integration points.

The pyramidal neuron is the basic computational unit of the cortex. Its distal tuft dendrite is heavily innervated by horizontal fibers coursing through layer 1 (L1), which provide long-range corticocortical and thalamocortical associational input (1–6). In the standard view of dendritic electogenesis of L5 pyramidal neurons, the basal and apical tuft dendrites are quite different (7–9). Whereas thin basal dendrites of neocortical pyramidal neurons initiate local *N*-methyl-D-aspartate (NMDA) and weak Na⁺ spikes (10–12), the apical dendrite is able to initiate calcium spikes (13–17). However, this view is based mostly on recordings from the thick apical dendrite, and little information is presently available with regard to the actual properties of the tuft dendrites, which are thin dendrites branching from the main bifurcation forming a tree that resembles more closely the

basal dendritic tree. It has been suggested that the properties that give rise to calcium spikes are restricted to an apical band (18) beyond which the initiation of Ca²⁺ spikes becomes progressively more difficult (19) [but see Rhodes and Llinás (20)]. This raises questions about the active and passive properties of the tuft dendrites, which are vital to understanding how and where feedback inputs to the pyramidal neuron are integrated (21). To overcome the difficulties in recording from these fine dendrites, we combined two-photon excitation fluorescence microscopy and infrared-scanning gradient contrast (10).

Using multiple simultaneous patch-clamp recordings from near the main apical bifurcation point (658 ± 110 µm from the soma; n = 28) and secondary and tertiary/quaternary tuft branches (775 ± 98 µm from the soma, n = 14; and 859 ± 60, n = 8) to within 50 µm of the pia of L5 pyramidal neurons, we directly tested the local spiking capabilities of fine tuft dendrites. Recordings from higher-order branches mostly in L1 or near the border of L1/L2 are referred to as “distal tuft” recordings. We first investigated local integration of synaptic input using visually guided focal stimulation at preselected distal tuft dendrites while recording simultaneously the voltage from nearby locations (Fig. 1A). Recordings

made from two distal tuft dendrites simultaneously while focally stimulating each of the branches revealed local, all-or-none spikes that failed to propagate to neighboring tuft branches (Fig. 1, B and C). On average, the spike attenuated by 86 ± 2.3% as it spread from one branch to another (n = 3).

Simultaneous recordings from distal and proximal tuft branches revealed that these all-or-none potentials originated in the fine distal tuft branches and attenuated as they spread proximally (Fig. 1, D to F). The voltage threshold for initiation of synaptically evoked dendritic spikes at the distal tuft branches was 9.67 ± 4.69 mV, and the amplitude of the spike at the distal tuft branch recording site was an additional 17.39 ± 5.87 mV from threshold and 27.07 ± 9.62 mV from baseline (22, 23). These spikes attenuated further as they spread toward the main bifurcation point (by a factor of 2.25 ± 0.58; n = 6; average distance between the recording sites 189 ± 74 µm) (Fig. 1F) but still could contribute substantial depolarization. The cable-filtered distal tuft dendritic spike attenuated on average to 7.74 ± 2.8 mV at the proximal tuft recording site.

Because of their localization to the activated branch, we considered the possibility that, similar to basal dendrites, the main regenerative current of the distal tuft dendrites is carried through the synaptic currents themselves, that is, NMDA receptor channels (11). The specific NMDA receptor blocker AP5 (100 µM) completely abolished the dendritic spike and linearized the relationship between the synaptic stimulus intensity and the excitatory postsynaptic potential (EPSP) amplitude observed under control conditions (n = 7) (Fig. 1, G to I). To rule out the possibility that blockade of NMDA receptors simply increased the threshold for local spikes, we also used ultraviolet (UV) laser uncaging of glutamate (MNI-glutamate) directed to a specific location in the distal tuft dendrites while recording the nearby dendritic voltage (recordings at 832 ± 61.5 µm from the soma passed second bifurcation and mostly at third bifurcations; uncaging site was 18 ± 2.7 µm distal to recording site; n = 8) (Fig. 1J) (24). Gradually increasing the UV laser intensity evoked gradual EPSP-like potentials until a threshold value

¹Department of Physiology, University of Berne, Bühlpark 5, 3012 Berne, Switzerland. ²Department of Physiology, The Rappaport Faculty of Medicine and Research Institute, Technion-Israel Institute of Technology, Bat-Galim, Haifa 31096, Israel.

*These authors contributed equally to this work.

†To whom correspondence should be addressed. E-mail: matthew.larkum@gmail.com (M.E.L.); jackie@tx.technion.ac.il (J.S.)

beyond which a spike was initiated (Fig. 1J). With this stimulation method, we could test the contribution of Na^+ and Ca^{2+} voltage-gate channels with application of tetrodotoxin (TTX) ($1 \mu\text{M}$), cadmium ($100 \mu\text{M}$), and nickel ($100 \mu\text{M}$). These blockers had only a minor effect on the spike amplitude and threshold (spike amplitude from baseline $53.5 \pm 7 \text{ mV}$ and $51.2 \pm 7.4 \text{ mV}$; spike threshold $18.7 \pm 4.1 \text{ mV}$ and $19.2 \pm 4.6 \text{ mV}$ before and after application of cadmium, nickel, and TTX, respectively; $n = 5$). In contrast, it was not possible to evoke a spike in the presence of AP5 ($50 \mu\text{M}$; $n = 4$).

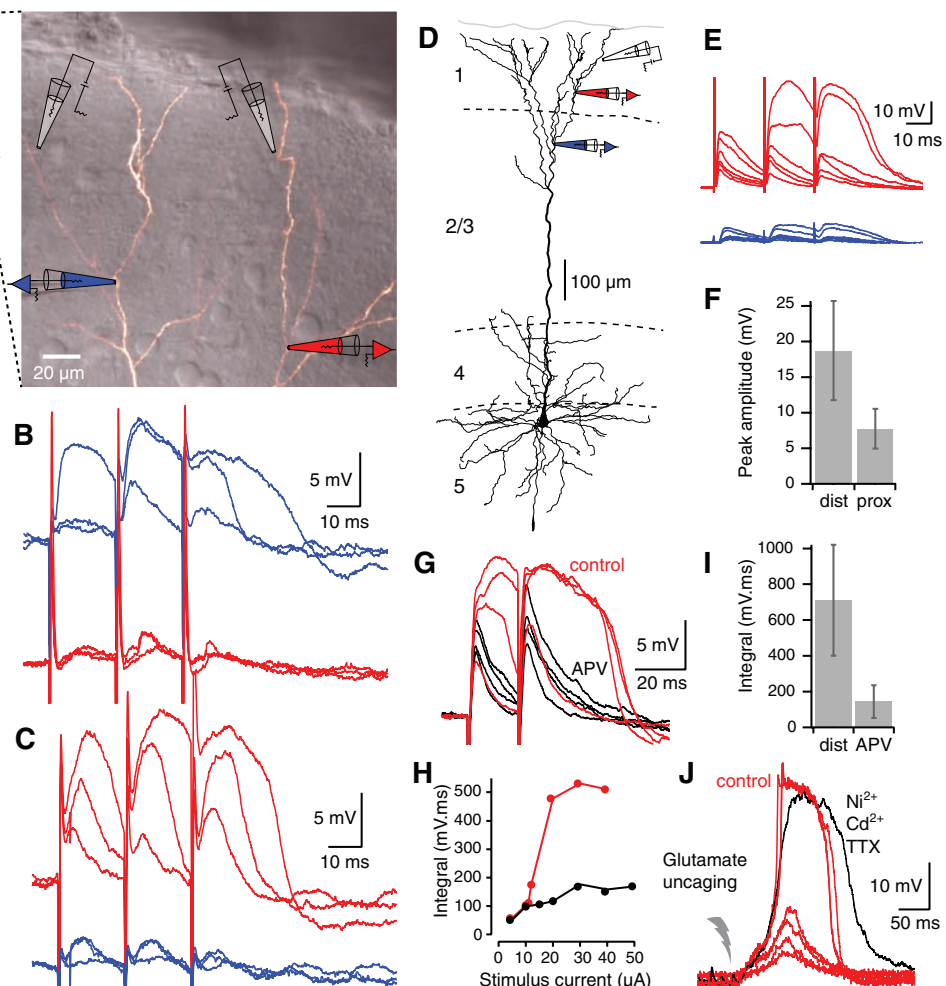
Our uncaging experiments suggested that distal tuft dendrites cannot support calcium electrogenesis but can support weak sodium spikes in addition to NMDA spikes. To further investigate

this point, we used direct current injection through dendritic patch electrodes (Fig. 2A). In agreement with previous reports (14, 19), current injection (300 pA to 1900 pA , 800 ms) to the proximal tuft dendrites (main bifurcation and primary tuft branches) nearly always initiated a calcium spike at the site of injection (Fig. 2, B and F) ($n = 39/43$; average threshold $1003 \pm 346 \text{ pA}$). These calcium spikes propagated well into the distal tuft branches (including to tertiary and quaternary branches), only attenuating to $92.6 \pm 7\%$ of the proximal tuft amplitude (see also fig. S1). In contrast, current injection to distal tuft dendrites rarely initiated dendritic Ca^{2+} spikes. In distal tuft branches, Ca^{2+} spikes were evoked in only 4 out of 36 cases (Fig. 2F). However, in 24 out of 36 recordings, small regenerative events

were initiated (average $20 \pm 7 \text{ mV}$ as measured from baseline; $n = 24$), and in the rest (8/36), no regenerative events could be elicited with up to 2400 pA current injection (Fig. 2F). The dichotomy between distal versus proximal electrogenesis was confirmed statistically using Fisher's exact test ($P < 0.001$). The threshold of the small regenerative event was $1008 \pm 475 \text{ pA}$ in secondary branches and $736 \pm 238 \text{ pA}$ in tertiary or more distal branches, and its forward propagation was poor (attenuation between 2 and 3 branch points to $33\% \pm 14\%$ of its original value; $n = 9$).

Addition of TTX ($1 \mu\text{M}$) (Fig. 2D) did not block the initiation of regenerative potentials at the proximal tuft dendrites [which in some cases even became longer (e.g., Fig. 2D, black)] but

Fig. 1. NMDA spikes in fine tuft dendrites of L5 pyramidal neurons. (A) Two-photon fluorescence image of an L5 pyramidal neuron (left) and fluorescence image overlaid with scanning gradient contrast image (right). (B and C) Parallel recordings were performed from two tuft dendrites simultaneously (blue electrode, 4th bifurcation, $975 \mu\text{m}$ from the soma; red electrode, 3rd bifurcation, $944 \mu\text{m}$ from the soma) while separately focally (gray electrodes) each of the recorded sub-branches sequentially with gradually increasing stimulus intensity until an NMDA spike was evoked. Simultaneous responses are shown from both locations, with increasing stimulation intensity near the blue electrode (B) and the red electrode (C). (D) Reconstruction of a biocytin-filled L5 pyramidal neuron showing the experimental setup. Dendritic recording pipettes are shown near the third bifurcation ($875 \mu\text{m}$ from the soma, red) and near the second bifurcation ($715 \mu\text{m}$ from the soma, blue). An extracellular stimulation electrode (black) was positioned $\sim 100 \mu\text{m}$ distal to the distal recording electrode. (E) Responses to gradual increase of the extracellular stimulus (from 4 to $9 \mu\text{A}$) recorded in both electrodes. (F) Summary of the size of extracellularly evoked dendritic spikes recorded in the distal tuft and proximal tuft shaft for six neurons (distance between the two recording electrodes $189.2 \pm 74 \mu\text{m}$). Peak responses were measured from threshold. (G) Dendritic recording from another pyramidal neuron after the second bifurcation ($807 \mu\text{m}$ from the soma, red), similar to the recording shown in (D). An extracellular synaptic stimulation electrode was positioned $\sim 100 \mu\text{m}$ from the recording



electrode. Gradually increasing extracellular stimulation strength (10 to $40 \mu\text{A}$) led to broad regenerative spikes that were blocked by the addition of $50 \mu\text{M}$ AP5. (H) Integral of the voltage responses to a paired stimulation before (red) and after application of AP5 for recordings shown in (G). The integral was measured over the entire response. (I) Summary of results in (G) and (H) showing the blockade of the spike by AP5. (J) Uncaging MNI-glutamate near another tuft dendrite (recording electrode $830 \mu\text{m}$ from the soma, uncaging $40 \mu\text{m}$ from recording site) also led to a prolonged spike (red) which was not blocked by a combination of $100 \mu\text{M}$ Ni^{2+} , $100 \mu\text{M}$ Cd^{2+} , and $1 \mu\text{M}$ TTX (black). Note the blockade of a small sodium component in the spike by TTX (black).

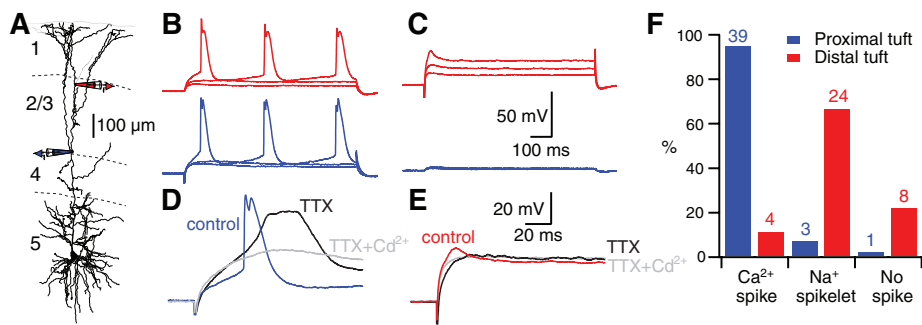


Fig. 2. Properties of the L5 pyramidal distal apical tuft dendrite revealed by current injection. **(A)** Reconstruction of biocytin-filled L5 pyramidal neuron showing the experimental setup. Two dendritic tuft recording pipettes are shown (blue electrode, 550 μm at main bifurcation point; red electrode at distal tuft, 850 μm from the soma). **(B)** Long current injection (400-ms steps) at the more proximal tuft electrode resulted in broad dendritic spikes first at the proximal (blue) and then distal (red) electrode. **(C)** Current injection at the distal tuft electrode (red) evoked only a small spikelet that did not propagate to the proximal tuft electrode (blue). **(D)** Suprathreshold spike response to same current injection shown in (B) in control conditions and after consecutive application of 1 μM TTX (black) and 100 μM Cd^{2+} (gray) to the extracellular solution. **(E)** Same as (D) for distal current injection. **(F)** Summary of responses to suprathreshold current injection in different L5 pyramidal cells when current was injected in dendrites of branch order 1 (blue, i.e., on or after the main bifurcation) compared with responses to injection in higher-order branches (red).

completely abolished the local regenerative events in distal tuft branches (Fig. 2E, red) ($n = 4$). Addition of extracellular cadmium (100 μM), however, blocked the regenerative event at the proximal tuft dendrites but had no further effect on the response seen in the distal tuft branches ($n = 4$) (Fig. 2E). Dendrite thickness was a good predictor of Na^+ spikelet versus Ca^{2+} spike electrogenesis, thicker ($3.0 \pm 1.1 \mu\text{m}$; $n = 26$) dendrites supporting calcium spikes and thinner ($1.6 \pm 0.5 \mu\text{m}$; $n = 19$) dendrites supporting pure sodium electrogenesis only (fig. S4).

Several properties, including the existence of local NMDA spikes and the weak electrogenesis of both sodium and calcium spikes, suggest that the relationship of the fine distal tuft branches to the apical Ca^{2+} initiation zone is similar to the relationship of the basal dendrites to the axosomatic initiation zone (10). However, one of the most notable remaining differences between the distal tuft and basal dendrites is the presence of hyperpolarization-activated current (I_h) (25–27). This current, which is active at resting potentials, acts like a leak and could potentially determine

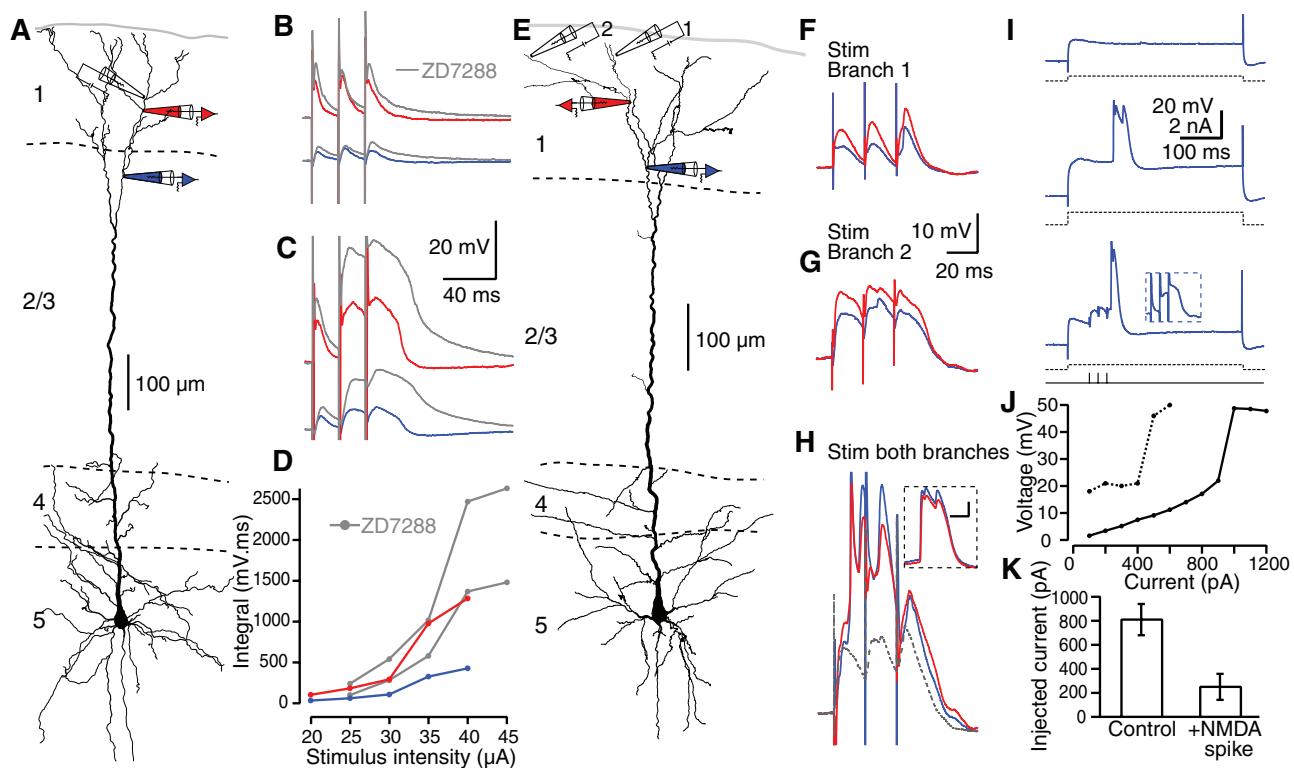


Fig. 3. Compartmentalization and interactions of NMDA spikes in the tuft. **(A to D)** Recordings were made from proximal tuft dendrite electrodes at 790 μm (blue) and at distal tuft dendrite 930 μm (red) from the soma (A). The effect of the I_h -channel blocker ZD7288 on the EPSPs (B) and NMDA spikes (C) evoked by extracellular synaptic stimulation (black electrode) at tuft dendrites. (D) Integral of the responses as a function of the stimulus intensity. For (B) to (D), colored traces show control responses, and gray traces indicate the same responses after application of ZD7288 (D). **(E to H)** Simultaneous activation of two tuft branches evoked a calcium spike. **(E)** Experimental setup. Simultaneous stimulation at site 1, which alone evoked an EPSP (F), and at site 2, which alone evoked an NMDA spike (G), summed and crossed the threshold in the calcium spike initiation zone (H). **(Inset)** The calcium spike evoked by current injection at the proximal electrode (no calcium spike could be evoked at the distal site, red). Recording electrodes at 640 μm (blue) and 750 μm (red) from the soma (E). **(I)** Subthreshold current injection (350 nA, top, black dashed line) in the calcium spike initiation zone (top, blue trace) reached threshold at 900 nA (middle), which was also reached by 350 nA current injection with a simultaneous NMDA spike in a branch (evoked at the 4th bifurcation and recorded at the 3rd bifurcation; reconstructed cell not shown). **(J)** Maximum depolarization in the presence (dashed line) and absence (solid line) of NMDA spike initiation at a third-order bifurcation. **(K)** Average current threshold at the site proximal to the main bifurcation site needed to evoke a Ca^{2+} spike with and without an NMDA spike.

completely abolished the local regenerative events in distal tuft branches (Fig. 2E, red) ($n = 4$). Addition of extracellular cadmium (100 μM), however, blocked the regenerative event at the proximal tuft dendrites but had no further effect on the response seen in the distal tuft branches ($n = 4$) (Fig. 2E). Dendrite thickness was a good predictor of Na^+ spikelet versus Ca^{2+} spike electrogenesis, thicker ($3.0 \pm 1.1 \mu\text{m}$; $n = 26$) dendrites supporting calcium spikes and thinner ($1.6 \pm 0.5 \mu\text{m}$; $n = 19$) dendrites supporting pure sodium electrogenesis only (fig. S4).

Several properties, including the existence of local NMDA spikes and the weak electrogenesis of both sodium and calcium spikes, suggest that the relationship of the fine distal tuft branches to the apical Ca^{2+} initiation zone is similar to the relationship of the basal dendrites to the axosomatic initiation zone (10). However, one of the most notable remaining differences between the distal tuft and basal dendrites is the presence of hyperpolarization-activated current (I_h) (25–27). This current, which is active at resting potentials, acts like a leak and could potentially determine

the degree of compartmentalization of the tuft tree and lead to substantial current loss of signals propagating toward the apical Ca^{2+} spike dendritic initiation zone. Addition of the I_h channel blocker ZD7288 to the bath solution (50 to 100 μM) led to an increase in the size and integral of NMDA spikes at both tuft dendrites and the main apical bifurcation point (Fig. 3, A to D). In the presence of ZD7288, the average amplitude of NMDA spikes increased by $221 \pm 35\%$ in the tuft and by $298 \pm 63\%$ ($n = 4$) in the proximal tuft dendrites. Our findings show that I_h currents had dramatic effects on the characteristics and spread of NMDA spikes, and thus on the degree of compartmentalization of the tuft tree.

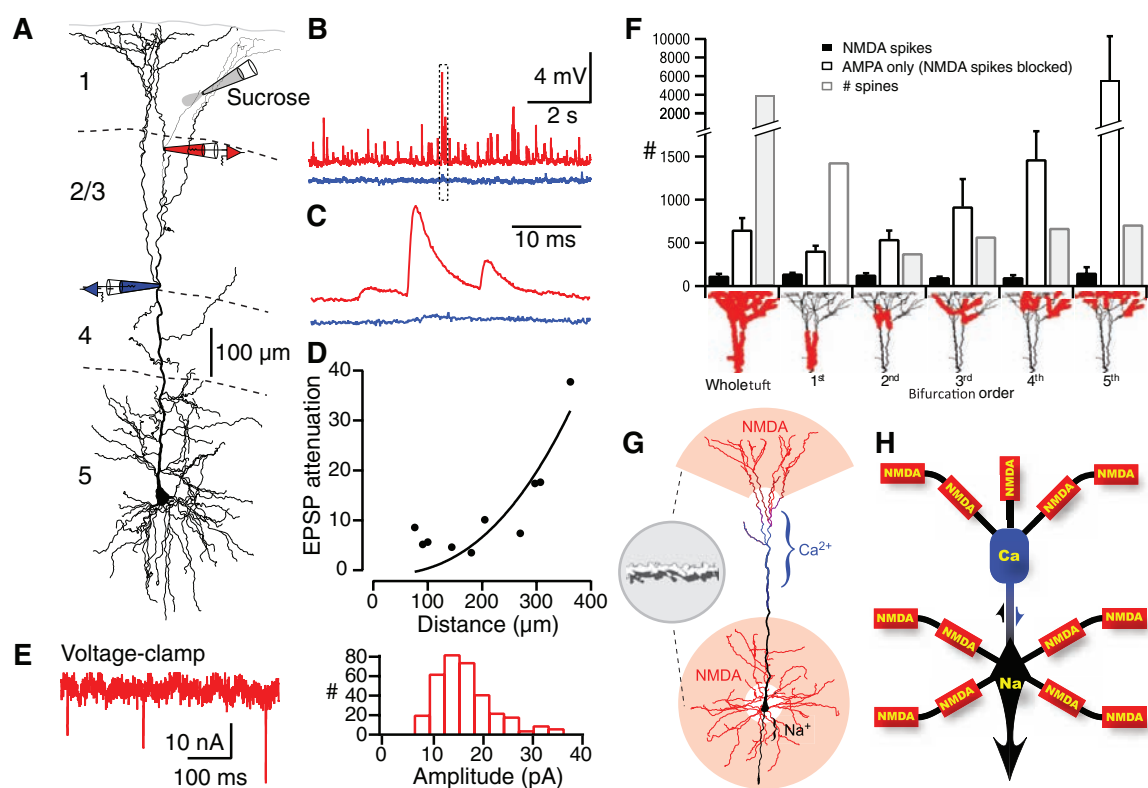
The calcium initiation zone is considered to be an integration zone conveying pre-integrated apical information to the axosomatic initiation zone (28–31). Thus, we were interested in the summation process of NMDA spikes at the level of the calcium spike initiation zone. The attenuation of the NMDA spike initiated at a single distal tuft branch meant that the threshold for a Ca^{2+} spike was never reached at the Ca^{2+} initiation zone by a single distal NMDA spike at threshold stimulation ($n = 20$) (32). However, the

voltage of two distal tuft branches could sum to initiate an apical calcium spike. Dual-site focal synaptic stimulation of identified thin tuft dendrites showed that the generation of NMDA spikes in two different distal tuft branches, or even an NMDA spike in one branch and an EPSP in the second, was sufficient to reach threshold at the Ca^{2+} initiation zone (Fig. 3, E to G; $n = 7$). Furthermore, small depolarization near the Ca^{2+} spike initiation zone enabled NMDA spikes in single distal tuft branches to evoke Ca^{2+} spikes (Fig. 3, I to K). Pairing current injections at the calcium initiation zone with NMDA spikes at distal tuft branches lowered significantly the current injection required for calcium spike initiation (current threshold changed from 820 ± 130 pA at control to 260 ± 108 pA during pairing; $P = 0.0001$).

How crucial are NMDA spikes in firing the calcium initiation zone? To evaluate the impact tuft inputs may have at the apical calcium spike initiation zone without the influence of NMDA spikes, we characterized the size and propagation of the unitary synaptic events at the distal tuft branches. Spontaneous and sucrose-evoked synaptic inputs to the distal tuft branches were severely attenuated after propagating to the cal-

cium spike initiation zone (Fig. 4, A to D). Next, we used computer simulations in the NEURON simulation platform to investigate the contribution of tuft NMDA spikes versus tuft AMPA-EPSPs in initiating apical calcium spikes. Active and passive parameters were varied until a good agreement with our experimental data was obtained (fig. S2). To fit the experimental data, voltage-gated potassium channel density in the tuft region was made an order of magnitude lower than the apical trunk. In addition, we inserted low calcium conductance into the tuft region, combined with a “hot zone” of calcium conductance situated at the main bifurcation zone extending 500 to 800 μm from the soma. When the calcium conductance was evenly distributed throughout the tuft, we could not fit the experimental data regardless of the amount of potassium conductance inserted. The model either could not evoke calcium spikes (low calcium) or evoked ripples (high calcium). Spine density was determined from reconstructed biocytin-labeled cells used in this study. The unitary synaptic conductance was estimated from both sucrose-evoked EPSPs and excitatory postsynaptic currents (EPSCs) (17.32 ± 8.6 pA) (Fig. 4, A to E), with

Fig. 4. General scheme for the integration of synaptic input to the tuft. (A) Reconstruction of biocytin-filled L5 pyramidal neuron showing the experimental setup. Two tuft recording pipettes are shown (blue electrode, 550 μm from the soma; red electrode, 850 μm from the soma). Another pipette for locally applying a high-sucrose solution is shown near a distal tuft branch (black, 915 μm from the soma.) (B) Spontaneous activity after local application of sucrose to the distal tuft. (C) Same as (B) for the time indicated by the box in (B). (D) Attenuation of EPSPs (spontaneous and sucrose-evoked pooled) versus distance from the distal (higher branch order) recording electrode to the proximal (first-order branch) electrode for 10 neurons. Here, zero marks the position of the proximal recording electrode. (E) Voltage-clamp recordings at a distal tuft branch 950 μm from the soma in a different neuron. (Left) Examples of unitary EPSCs evoked by local sucrose application (10 μm distal to the recording site). (Right) Amplitude histogram distribution of unitary EPSC from the same recording (175 events). (F) Results of simulations in NEURON predicting the number of active synapses at the tuft needed to generate a Ca^{2+} spike near the main bifurcation point (activated randomly at different locations). The results are binned according to the region with active synapses (shown schematically underneath). Indicated for each bin is the number of active synapses required under control



marks the position of the proximal recording electrode. (E) Voltage-clamp recordings at a distal tuft branch 950 μm from the soma in a different neuron. (Left) Examples of unitary EPSCs evoked by local sucrose application (10 μm distal to the recording site). (Right) Amplitude histogram distribution of unitary EPSC from the same recording (175 events). (F) Results of simulations in NEURON predicting the number of active synapses at the tuft needed to generate a Ca^{2+} spike near the main bifurcation point (activated randomly at different locations). The results are binned according to the region with active synapses (shown schematically underneath). Indicated for each bin is the number of active synapses required under control

conditions (NMDA spikes, black), without NMDA receptors (AMPA only, white), and also the total number of spines per activated region (gray). (G) Reconstructed pyramidal neuron showing the regions of the dendritic tree where NMDA (red), Ca^{2+} (blue), and Na^+ (black) electrogenesis can be initiated. (Inset) Enlargement of typical thin branch with a higher density of synapses than thicker dendrites (33). (H) Schematic representation of the important subcompartments of a typical L5 pyramidal neuron showing the relationship of multiple local sites for NMDA spikes to the Ca^{2+} and Na^+ initiation zones, which can signal each other through active propagation along the main apical trunk (arrows).

4.25 ± 1.9 pA of NMDA current at resting membrane potential. In addition, we measured directly (830 to 950 μm from the soma) the total and NMDA just-suprathreshold current needed for NMDA spike initiation using glutamate uncaging (total current of 187 ± 43 pA; NMDA current of 88 ± 19 pA; $n = 5$) (fig. S2D). Using these parameters, NMDA spikes could be initiated at all locations on the tuft tree; however, the number of synapses needed was far lower in the very distal tuft branches. Just 8.75 ± 2.21 synapses were needed to evoke NMDA spikes near the ends of the tuft branches, whereas up to 43 ± 4.54 synapses were needed at 250 μm from the pia, leading to a depolarization of 1.07 ± 0.25 mV and 9.22 ± 1.4 mV, respectively, at the calcium spike initiation zone (fig. S2). The contribution of voltage-gated calcium channels was negligible at the tuft regions (fig. S2) but became prominent at the apical calcium initiation zone (extending ~ 340 μm from the first bifurcation), where a full-blown calcium spike was evoked (fig. S2).

When we activated randomly distributed synapses at the tuft dendrites, which usually leads to NMDA spike initiation at multiple branches, we found that 116.66 ± 25.59 randomly distributed synapses (2.9% of total synapses) over the whole tuft region are sufficient to trigger a calcium spike (Fig. 4F). Interestingly, when we redistributed the activated synapses based on bifurcation order, calcium spikes were most readily initiated by third- and fourth-order branches (100.83 ± 11.64 and 99 ± 28.75 synapses, respectively) (Fig. 4F). Blocking NMDA receptors caused a dramatic increase in the number of synapses at tuft branches needed for calcium spike initiation. In this scenario, the number of synapses increased exponentially with branch order, from 408.33 ± 59.69 synapses near the main bifurcation to 5550 ± 4749 synapses at the terminal branches (exceeding the total spine number at these dendrites) (33) (Fig. 4F). In contrast, NMDA spikes only modestly contributed to the initiation of calcium spikes when synapses were activated at the calcium initiation zone itself (Fig. 4F, first bifurcation). On the other hand, uniformly increasing calcium conductance in tuft branches (up to a factor of 3) did not change the requirement for an exponential increase in the number of pure AMPA synapses needed to initiate a calcium spike at the main bifurcation point.

Thus, there are three stages (thresholds) in the integration of top-down associative information terminating at distal tuft branches: (i) NMDA spike initiation at the distal tuft branches, (ii) Ca^{2+} spike initiation near the main bifurcation, and (iii) sodium spike initiation at the axon hillock (Fig. 4, G and H).

Taking all the properties together, a new unifying principle emerges as to how pyramidal neurons integrate synaptic information. The thin distal tuft and basal dendrites of pyramidal neurons, which receive the overwhelming majority of synaptic inputs (33), appear to constitute a class of dendrite in which NMDA spikes are the predominant regenerative events summing synaptic inputs in semi-independent compartments.

The output of each subunit in this class of dendrite is passed on to the major sites of integration at the axon and apical calcium initiation zones, which can all interact via actively propagated signals (34), enabling the interactions between top-down and bottom-up information.

References and Notes

- D. J. Felleman, D. C. Van Essen, *Cereb. Cortex* **1**, 1 (1991).
- K. S. Rockland, D. N. Pandya, *Brain Res.* **179**, 3 (1979).
- J. M. Budd, *Proc. R. Soc. London Ser. B Biol. Sci.* **265**, 1037 (1998).
- B. Kuhn, W. Denk, R. M. Bruno, *Proc. Natl. Acad. Sci. U.S.A.* **105**, 7588 (2008).
- L. Petreanu, T. Mao, S. M. Sternson, K. Svoboda, *Nature* **457**, 1142 (2009).
- P. Rubio-Garrido, F. Pérez-de-Manzo, C. Porrero, M. J. Galazo, F. Clascá, *Cereb. Cortex*; published online 2 February 2009 (10.1093/cercor/bhn259).
- O. Bernander, C. Koch, R. J. Douglas, *J. Neurophysiol.* **72**, 2743 (1994).
- M. Häusser, N. Spruston, G. J. Stuart, *Science* **290**, 739 (2000).
- N. Spruston, *Nat. Rev. Neurosci.* **9**, 206 (2008).
- T. Nevanian, M. E. Larkum, A. Polksy, J. Schiller, *Nat. Neurosci.* **10**, 206 (2007).
- J. Schiller, G. Major, H. J. Koester, Y. Schiller, *Nature* **404**, 285 (2000).
- B. A. Milojkovic, J. P. Wuskell, L. M. Loew, S. D. Antic, *J. Membr. Biol.* **208**, 155 (2005).
- H. G. Kim, B. W. Connors, *J. Neurosci.* **13**, 5301 (1993).
- J. Schiller, Y. Schiller, G. Stuart, B. Sakmann, *J. Physiol. London* **505**, 605 (1997).
- M. E. Larkum, K. M. Kaiser, B. Sakmann, *Proc. Natl. Acad. Sci. U.S.A.* **96**, 14600 (1999).
- M. E. Larkum, J. J. Zhu, B. Sakmann, *Nature* **398**, 338 (1999).
- A. Polksy, B. W. Mel, J. Schiller, *Nat. Neurosci.* **7**, 621 (2004).
- R. Yuste, M. J. Gutnick, D. Saar, K. R. Delaney, D. W. Tank, *Neuron* **13**, 23 (1994).
- M. E. Larkum, J. J. Zhu, *J. Neurosci.* **22**, 6991 (2002).
- P. A. Rhodes, R. R. Llinás, *J. Physiol.* **536**, 167 (2001).
- S. R. Williams, G. J. Stuart, *Trends Neurosci.* **26**, 147 (2003).
- J. Bullier, *Brain Res. Brain Res. Rev.* **36**, 96 (2001).
- The dendritic spike was probably larger than this at the site of initiation, which was most likely closer to the stimulating electrode.
- Distal dendritic recording sites were chosen on the basis of dendrite thickness and the lack of Ca^{2+} spike initiation.
- T. Berger, M. E. Larkum, H. R. Lüscher, *J. Neurophysiol.* **85**, 855 (2001).
- S. R. Williams, G. J. Stuart, *J. Neurophysiol.* **83**, 3177 (2000).
- A. Lörincz, T. Notomi, G. Tamás, R. Shigemoto, Z. Nusser, *Nat. Neurosci.* **5**, 1185 (2002).
- P. A. Rhodes, in *Cerebral Cortex, Vol. 13*, P. S. Ulinski, E. G. Jones, A. Peters, Eds. (Plenum, New York, 1999), pp. 139–200.
- C. Koch, I. Segev, *Nat. Neurosci.* **3** (suppl.), 1171 (2000).
- N. Spruston, W. L. Kath, *Nat. Neurosci.* **7**, 567 (2004).
- M. London, M. Häusser, *Annu. Rev. Neurosci.* **28**, 503 (2005).
- With the I_h -blocker ZD7288, single NMDA spikes sometimes caused Ca^{2+} spikes.
- A. U. Larkman, *J. Comp. Neurol.* **306**, 332 (1991).
- M. E. Larkum, J. J. Zhu, B. Sakmann, *J. Physiol. London* **533**, 447 (2001).
- We thank B. Sakmann for generous support and comments on the manuscript and Y. Schiller for helpful comments and discussions on the manuscript. We thank K. Fischer for NeuroLucida reconstructions of the biocytin-filled neurons. This study was supported by NIH, the Israel Science Foundation, and the Rappaport Foundation (J.S.); by the Swiss National Science Foundation (M.L., grant PPO03-119159; T.N., grant 3100A0-118395); and by SystemsX.ch (M.L., Neurochoice). The authors declare that they have no competing financial interests.

Supporting Online Material

www.sciencemag.org/cgi/content/full/325/5941/756/DC1

Materials and Methods

Figs. S1 to S4

References

6 February 2009; accepted 24 June 2009

10.1126/science.1171958

Spinal Endocannabinoids and CB_1 Receptors Mediate C-Fiber–Induced Heterosynaptic Pain Sensitization

Alejandro J. Pernía-Andrade,^{1,*†} Ako Kato,^{1,9*} Robert Witschi,^{1,9} Rita Nyilas,²

István Katona,² Tamás F. Freund,² Masahiko Watanabe,³ Jörg Filitz,⁴ Wolfgang Koppert,^{4†} Jürgen Schüttler,⁴ Guangchen Ji,⁵ Volker Neugebauer,⁵ Giovanni Marsicano,⁶ Beat Lutz,⁷ Horacio Vanegas,⁸ Hanns Ulrich Zeilhofer,^{1,9§}

Diminished synaptic inhibition in the spinal dorsal horn is a major contributor to chronic pain. Pathways that reduce synaptic inhibition in inflammatory and neuropathic pain states have been identified, but central hyperalgesia and diminished dorsal horn synaptic inhibition also occur in the absence of inflammation or neuropathy, solely triggered by intense nociceptive (C-fiber) input to the spinal dorsal horn. We found that endocannabinoids, produced upon strong nociceptive stimulation, activated type 1 cannabinoid (CB_1) receptors on inhibitory dorsal horn neurons to reduce the synaptic release of γ -aminobutyric acid and glycine and thus rendered nociceptive neurons excitable by nonpainful stimuli. Our results suggest that spinal endocannabinoids and CB_1 receptors on inhibitory dorsal horn interneurons act as mediators of heterosynaptic pain sensitization and play an unexpected role in dorsal horn pain-controlling circuits.

Activity-dependent central hyperalgesia can be induced in the absence of any inflammation or nerve damage by selective activation of glutamatergic C-fiber nociceptors; for example, with the specific transient receptor potential channel (TRP) V1 agonist capsaicin.

Local subcutaneous injection of capsaicin induces primary hyperalgesia at the site of injection and a purely mechanical secondary hyperalgesia in the surrounding healthy skin (1). This secondary hyperalgesia originates from changes in the central processing of input from mechano-